

Manganese Oxides | Hot Paper |

Water Oxidation Catalysis by Synthetic Manganese Oxides with Different Structural Motifs: A Comparative Study

Carolin E. Frey and Philipp Kurz^{*[a]}

Abstract: Manganese oxides are considered to be very promising materials for water oxidation catalysis (WOC), but the structural parameters influencing their catalytic activity have so far not been clearly identified. For this study, a dozen manganese oxides (MnO_x) with various solid-state structures were synthesised and carefully characterised by various physical and chemical methods. WOC by the different MnO_x was then investigated with Ce^{4+} as chemical oxidant. Oxides with layered structures (birnessites) and those containing large tunnels (todorokites) clearly gave the best results with reaction rates exceeding $1250 \text{ mmolO}_2 \text{ mol}_{\text{Mn}}^{-1} \text{ h}^{-1}$ or about $50 \mu\text{molO}_2 \text{ m}^{-2} \text{ h}^{-1}$. In comparison, catalytic rates per

mole of Mn of oxides characterised by well-defined 3D networks were rather low (e.g., ca. $90 \text{ mmolO}_2 \text{ mol}_{\text{Mn}}^{-1} \text{ h}^{-1}$ for bixbyite, Mn_2O_3), but impressive if normalised per unit surface area ($> 100 \mu\text{molO}_2 \text{ m}^{-2} \text{ h}^{-1}$ for marokite, CaMn_2O_4). Thus, two groups of MnO_x emerge from this screening as hot candidates for manganese-based WOC materials: 1) amorphous oxides with tunnelled structures and the well-established layered oxides; 2) crystalline Mn^{III} oxides. However, synthetic methods to increase surface areas must be developed for the latter to obtain good catalysis rates per mole of Mn or per unit catalyst mass.

Introduction

The future of the world's energy supply is renewable energy. In 2012, an estimated 19% of the world's energy consumption was renewable energy, and the prediction for 2013 was even higher.^[1] A disadvantage of most renewable energy sources is that production cannot easily be regulated to meet demand. Therefore, technologies to store large amounts of renewable energy are needed. The splitting of water into hydrogen and oxygen is one of the prominent concepts for this task, since the produced H_2 could be used as a storable and environmentally friendly fuel. To make this reaction economically feasible, a central problem to be solved is the development of an affordable, abundant and non-toxic catalyst for the oxidation of water to dioxygen, a reaction that is central to all such renewable-fuel schemes.

In biology, water oxidation takes place at the oxygen-evolving complex (OEC) of the photosystem II (PSII) enzyme complex.^[2] The OEC consist of a CaMn_4O_5 cluster embedded in an amino acid environment.^[2,3] The metal ions of the OEC are interconnected by μ -oxido bridges, and the Mn oxidation states switch between Mn^{3+} and Mn^{4+} in the catalytic cycle, which involves four single-electron transfer steps.^[4,5]

In artificial, bio-inspired systems for water splitting, manganese oxides (MnO_x) have been used as materials for water oxidation catalysis (WOC) since the late 1960s.^[6–8] This approach has been “rediscovered” in recent years, and it has been found that good WOC rates can especially be obtained if MnO_x from the so-called birnessite family of oxides are used as heterogeneous, Mn-based catalyst materials.^[8–13] Birnessites are manganese oxides containing layers of $[\text{MnO}_6]$ octahedra. The interlayer distance is approximately 7 Å and the average Mn oxidation state is in the range of +3.5–3.9.^[14–16] Varying amounts of water and secondary cations (especially of group 1 and 2 metals) can be incorporated into the interlayer space, and in consequence a large variety of birnessites with different chemical compositions are synthetically accessible.^[8,15] We and a number of other groups have used this compositional flexibility of birnessite-type MnO_x materials in recent years to optimise their WOC activities, and significant progress has been made, especially by variations of oxide compositions, sintering temperatures and particle sizes of synthetic birnessites. However, a large number of other manganese oxides with different solid-state structures is known (more than 30 types have been described;^[14] see Figure 1 for examples), but differences in WOC activities between these oxide types have rarely been studied. Hence, in this work, we prepared and investigated a dozen MnO_x materials with different compositions and structures in order to establish trends in catalytic activities. By doing so, we hoped to find new leads for promising MnO catalysts, as well as to obtain a better understanding of why birnessites have so far dominated the field of Mn-based WOC.

A range of different types of manganese oxides have already been tested for WOC, albeit rarely under identical experimental

[a] C. E. Frey, Prof. Dr. P. Kurz
Albert-Ludwigs-Universität Freiburg
Institut für Anorganische und Analytische Chemie
Albertstrasse 21, 79106 Freiburg (Germany)
E-mail: philipp.kurz@ac.uni-freiburg.de

Supporting information for this article is available on the WWW under <http://dx.doi.org/10.1002/chem.201501367>.

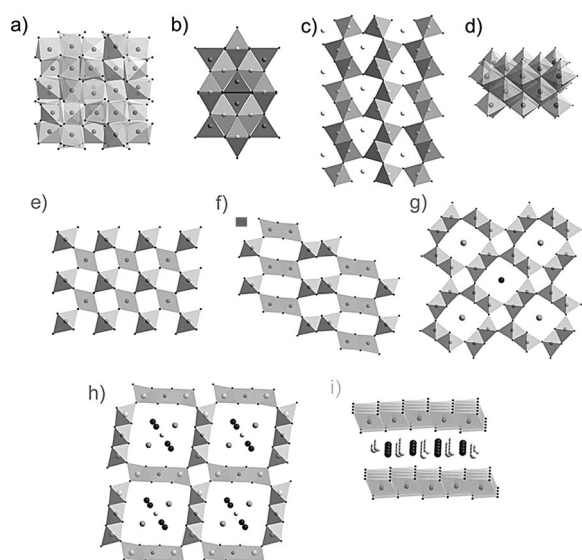


Figure 1. Structural motifs of some common manganese oxides.^[14] Networks (black labels): a) bixbyite (Mn_2O_3); b) spinel-type (hausmannite (Mn_3O_4), LiMn_2O_4); c) marokite (CaMn_2O_4); d) manganosite (MnO). Tunnelled structures (grey labels): e) pyrolusite, (MnO_2); f) ramsdellite; g) hollandite-group; h) todorokite. Layered oxides (light grey labels): i) birnessite group. Colour code: black = oxide (O^{2-}) or O of $\text{OH}^-/\text{H}_2\text{O}$; grey octahedra/tetrahedral = manganese; white = calcium or magnesium; light grey = potassium or sodium.

conditions.^[6,8,12,13,17–23] Instead, catalyst concentrations, oxidising agents, pH regime and so forth differed greatly from study to study, and the reported WOC rates therefore can hardly be compared. To our knowledge, in only one report to date have WOC rates of more than three different types of manganese oxide been screened in the same catalysis set-up, namely, the report by Robinson et al. in 2013 on a set of crystalline MnO_x compounds and their WOC performances.^[20] Robinson et al. first determined the identity of the synthetic oxides by XRD, analysed the surface areas by gas-sorption experiments and then screened catalytic activities with photogenerated $[\text{Ru}(\text{bpy})_3]^{3+}$ ($\text{bpy} = 2,2'$ -bipyridine) as oxidising agent. Reaction rates were normalised to catalyst surface area, and bixbyite (Mn_2O_3) was found to be the most active catalyst. In comparison, slow WOC was observed for hausmannite (Mn_3O_4) and synthetic λ - MnO_2 (a spinel-type oxide). Five other oxides were found to be inactive in WOC. This study focused on crystalline manganese oxides of well-defined composition, but these represent only a small fraction of the known MnO_x compounds. Herein, we therefore extend the investigation to less-ordered materials and present a systematic WOC analysis for twelve different MnO_x oxides in which crystalline and amorphous oxides of very different structures were screened by a common experimental procedure. Surprisingly, such a screening is so far lacking in the otherwise very active field of WOC by MnO_x .

For a short overview of common manganese oxide structures, some important manganese oxide phases are briefly described in the following. For more detailed information, see review articles on this topic.^[14,24]

Manganese oxides are often categorised into three different structure types, all of which contain $[\text{MnO}_6]$ units as basic

building blocks (Figure 1). The first group of manganese oxides can be summarised as crystalline, 3D networks of $\text{Mn}^{2+/3+/4+}$ and O^{2-} ions. Bixbyite (α - Mn_2O_3), hausmannite (Mn_3O_4) and LiMn_2O_4 (both spinel-like oxides), marokite (CaMn_2O_4) as well as manganosite (MnO , NaCl structure) are typical representatives of this group.

In the second structural type, $[\text{MnO}_6]$ octahedra are arranged in the form of tunnels. These tunnelled oxides can be subdivided by their tunnel architectures (e.g., $[2 \times 1]$, $[3 \times 3]$; see Figure 1), which also influence the amount of secondary cations and/or water that can be incorporated into the tunnelled structures. The average oxidation state of manganese here is usually between +3.0 and +4.0, and pyrolusite, ramsdellite, hollandite, cryptomelane and todorokite are common examples of this class.

A third class of manganese oxides are layered minerals. Prominent examples are birnessites, which form a large subgroup of compounds in the class of layered Mn oxides, and vernadite (δ - MnO_2). Layered MnO_x materials tend to be highly amorphous, and so details about their structures are often not known at the atomic level. However, common features of layered manganese oxides are interlayer distances of 7–10 Å, significant amounts of intercalated secondary cations and water and average manganese oxidation states of +3.5 to +4.0.

Given this large variety of solid-state structures and the known WOC activity of some manganese oxides, different factors have been suggested to be important for the catalytic process: 1) similar to the OEC, flexible structures should be beneficial for substrate binding and oxidation-state changes,^[5,9,10,12,18] 2) high surface areas result in good accessibility of the catalytically active centres,^[7,12,13,19,20,25] 3) average Mn oxidation states greater than +3.5 often provide enough thermodynamic driving force for water oxidation,^[7,18,22,26] 4) secondary cations such as (Lewis acidic) Ca^{2+} assist water oxidation by activation of the H_2O substrate^[10,12,13] and 5) good conductivity of the oxide enhances performance, because WOC requires that four oxidation equivalents accumulate at the (so far unidentified) catalytic sites in the MnO_x .^[9,18] Some of these factors are obviously contradictory to each other, and so there is currently no real consensus on the most important structural parameters influencing WOC activities of manganese oxides.

Therefore, we synthesised a representative variety of MnO_x compounds from the different structural types to probe the role of the type of manganese oxide in water oxidation. Suitable synthetic routes to the different phases were identified, and the different MnO_x products were first carefully characterised by a variety of analytical methods. Ion chromatography (IC) in combination with redox titration was used to determine the ion contents and average Mn oxidation states. From these values, the chemical composition of the oxides could be calculated. XRD and IR spectroscopy provided information about the atomic structure, crystallinity and water content of the samples. Surface areas as well as particle shapes and sizes were probed by nitrogen sorption and SEM. In combination with WOC runs using the well-established chemical Ce^{4+} system, we are thus able to present a very detailed dataset on

probably the most diverse series of MnO_x water oxidation catalysts screened in a single study so far.

Results and Discussion

Synthesis of manganese oxides

The three classes of manganese oxides are by now well described, and many synthetic procedures leading to the various oxides of each type have been reported. Since the main motivation of our work was the identification of catalysts for possible large-scale applications, we selected established MnO_x synthesis routes for this study that yield the desired products from low-cost precursors in simple procedures. If precipitation reactions led to the desired product, we chose routes that involve only aqueous media, because water is the solvent and substrate of WOC, and we thus hoped to obtain water-stable MnO_x samples.

Table 1 gives an overview of the used synthetic routes. Interestingly, one finds some general differences in the reaction conditions leading to the different oxide types. Nearly all preparations start from Mn^{II} precursors, but those of 3D networks commonly involve a final high-temperature calcination step, tunnelled structures are mainly the products of precipitation reactions at elevated temperatures and pressures (hydrothermal synthesis) and layered oxides are usually synthesised by $\text{Mn}^{\text{II}}/\text{Mn}^{\text{VII}}$ comproportionation reactions in water at room temperature.

Thus, the systematics of the MnO_x solid-state structures (Figure 1) are to some degree mirrored by the reaction conditions under which these oxides are typically formed.^[8]

XRD and IR spectroscopy

The synthetic procedures shown in Table 1 all yield powders with the brown to black colours typical of manganese oxides (see the Supporting Information, Figure S1). A first indication

of the actual MnO_x phase can be obtained from XRD measurements on these products (Figure 2 and the Supporting Information, Figure S2). For crystalline oxides, a correlation to the theoretical diffractograms is mostly straightforward and thus the products of the syntheses of bixbyite, hausmannite, LiMn_2O_4 , marokite, pyrolusite, cryptomelane and hollandite as well as the commercial sample of manganosite could all clearly be identified as the correct oxide phases. On the other hand, the XRD patterns of the products of the syntheses of tunnelled

Table 1. Synthetic routes for the preparations of the different manganese oxides investigated in this study. The chemical formulae given below the mineral names are generalised according to ref. [14]. For precise values of the products, see Table 2.

Manganese oxide	Synthesis	Ref.
bixbyite (Mn_2O_3)	$\text{MnCO}_3 \xrightarrow[\text{600}^\circ\text{C, 24 h}]{\text{Air}}$ bixbyite	[27]
hausmannite (Mn_3O_4)	$\text{MnCO}_3 \xrightarrow[\text{1000}^\circ\text{C, 24 h}]{\text{Air}}$ hausmannite	[27]
LiMn_2O_4	$\text{Mn(OAc)}_2 + \text{LiNO}_3 \xrightarrow[\text{HNO}_3, \text{H}_2\text{O, RT}]{\text{Urea, citric acid}}$ $\text{LiMn}_2\text{O}_4 \xrightarrow[\text{350}^\circ\text{C, 24 h}]{} \text{LiMn}_2\text{O}_4$	[28]
marokite (CaMn_2O_4)	$\text{Mn(OAc)}_2 + \text{Ca(NO}_3)_2 + \text{KMnO}_4 \xrightarrow[\text{H}_2\text{O}]{\text{KOH, RT}}$ Ca-birnessite $\xrightarrow[\text{1000}^\circ\text{C, 24 h}]{} \text{marokite}$	[17]
pyrolusite (MnO_2)	$\text{Mn(OAc)}_2 + \text{KMnO}_4 \xrightarrow[\text{H}_2\text{O, RT}]{\text{KOH}}$ K-birnessite $\xrightarrow[\text{H}_2\text{O}]{2^*\text{LiCl, RT}}$ Li-birnessite $\xrightarrow[\text{LiCl, H}_2\text{SO}_4]{\text{pyrolusite}}$ pyrolusite $\xrightarrow[\text{H}_2\text{O; autoclave, 150}^\circ\text{C, 48 h, } p = 6.3 \text{ bar}]{\text{LiCl, H}_2\text{SO}_4}$ pyrolusite	[29]
ramsdellite (MnO_2)	$\text{MnSO}_4 \xrightarrow[\text{H}_2\text{O; autoclave, 85}^\circ\text{C, 12 h, } p = 1.9 \text{ bar}]{(\text{NH}_4)_2\text{S}_2\text{O}_8}$ ramsdellite	[29]
cryptomelane [$\text{K}_x(\text{Mn}^{3+}, \text{Mn}^{4+})_8\text{O}_{16}$]	$\text{MnSO}_4 + \text{KMnO}_4 \xrightarrow[\text{H}_2\text{O, 110}^\circ\text{C, 24 h}]{\text{HNO}_3}$ cryptomelane	[30,31]
hollandite ($\text{MnO}_2 \cdot n\text{H}_2\text{O}$)	$\text{Mn}_2\text{O}_3 \xrightarrow[\text{H}_2\text{O, 80}^\circ\text{C, 6 h}]{\text{H}_2\text{SO}_4}$ cation-free hollandite	[20,32]
todorokite [$(\text{Ca}, \text{Na}, \text{K})_x(\text{Mn}^{3+}, \text{Mn}^{4+})_6\text{O}_{12} \cdot n\text{H}_2\text{O}$]	$\text{Mn(OAc)}_2 + \text{Ca(OAc)}_2 + \text{KMnO}_4 \xrightarrow[\text{H}_2\text{O; autoclave, 150}^\circ\text{C, 48 h, } p = 6.3 \text{ bar}]{\text{KOH, RT}}$ Ca-birnessite $\xrightarrow{} \text{todorokite}$	[15]
Ca-birnessite [$(\text{Ca}, \text{Na})_x(\text{Mn}^{3+}, \text{Mn}^{4+})_7\text{O}_{14} \cdot n\text{H}_2\text{O}$]	$\text{Mn(OAc)}_2 + \text{Ca(OAc)}_2 + \text{KMnO}_4 \xrightarrow[\text{H}_2\text{O}]{\text{KOH, RT}}$ Ca-birnessite	[9]
vernadite ($\text{MnO}_2 \cdot n\text{H}_2\text{O}$)	$\text{MnCl}_2 + \text{KMnO}_4 \xrightarrow[\text{H}_2\text{O, RT}]{\text{NaOH}}$ vernadite	[33]

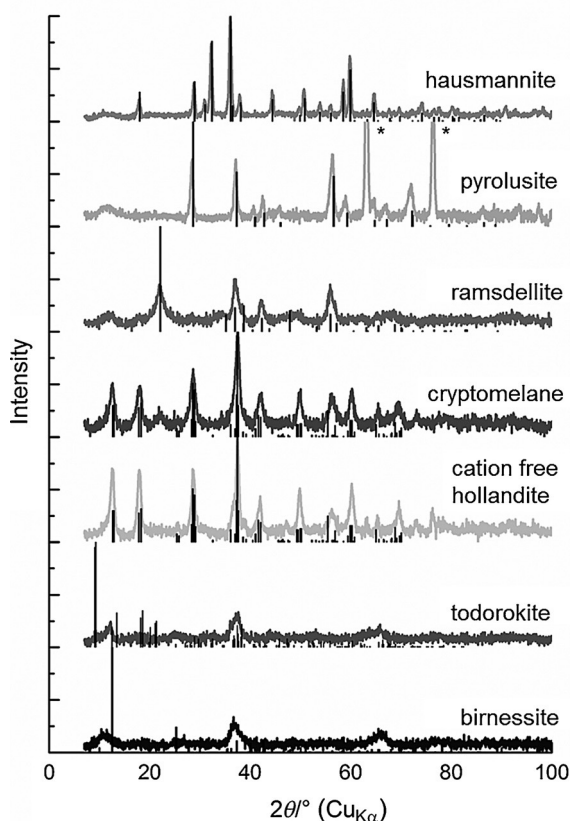


Figure 2. Powder XRD patterns for different synthetic manganese oxides. In each case, the theoretical patterns are shown as black bar graphs. Stars mark reflections originating from the aluminium sample holders. Additional diffractograms can be found in the Supporting Information, Figure S2.

or layered MnO_x are as expected rather featureless, because it is known that such oxides show only very little long-range order. Hence, it is not possible to assign the oxide phases of the isolated materials for ramsdellite, todorokite, birnessite and vernadite from the XRD data alone, and especially for these compounds further analytical methods must be employed to identify oxide type and composition.

ATR-IR spectra were recorded for all synthetic oxides (Figure 3 and the Supporting Information, Figure S3) and show bands in three ranges: $500\text{--}700\text{ cm}^{-1}$, around 1600 cm^{-1} and around 3300 cm^{-1} . For all Mn^{3+} - and/or Mn^{4+} -containing compounds, the most intense signals are the Mn–O vibrations in the range of $500\text{--}700\text{ cm}^{-1}$. These originate from deformations of the $[\text{MnO}_6]$ units and clearly differ between the individual MnO_x .^[34] Amorphous oxides such as birnessite and todorokite show broad bands, but sharp and defined signals are detected for crystalline materials such as hausmannite. The Mn–O stretching frequency of the Mn^{II} oxide manganosite is about 300 cm^{-1} ^[34] and was thus out of the range of our diamond ATR-IR set-up (lower detection limit: 500 cm^{-1}).

The IR bands at higher wavenumbers ($1500\text{--}1700\text{ cm}^{-1}$ and $3000\text{--}3600\text{ cm}^{-1}$) are associated with lattice water molecules or hydroxide ions,^[35] and it is well known that $\text{H}_2\text{O}/\text{OH}^-$ between layers or in tunnels of certain MnO_x cause IR absorptions in

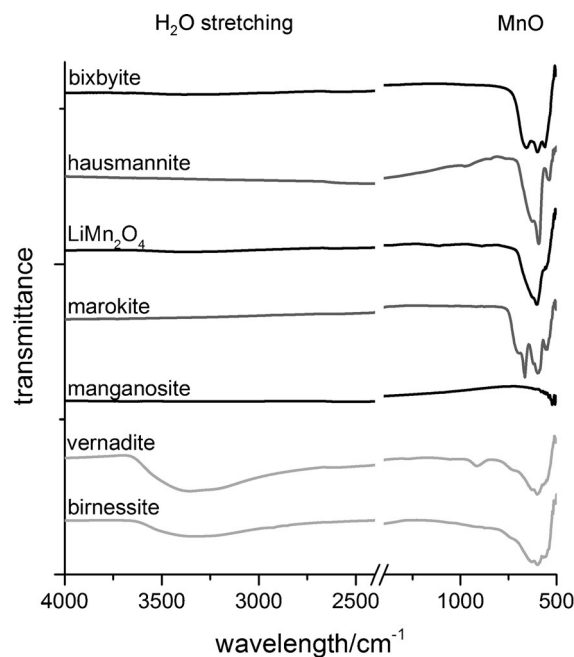


Figure 3. FTIR spectra for selected synthetic manganese oxides focussing on the spectral regions of the water and Mn–O bond stretching frequencies. Additional FTIR spectra are shown in the Supporting Information, Figure S2.

these regions.^[34] This interpretation is also in good agreement with our analyses of the chemical compositions of the oxides (see below): the water-related IR features are absent in the spectra of crystalline, 3D-network materials (only O^{2-} , but no $\text{H}_2\text{O}/\text{OH}^-$, in these structures; see Table 2), whereas we found pronounced water/hydroxide bands for layered oxides and compounds containing large tunnels. The intensities of these signals are also useful to confirm the relative amount of water in the materials calculated from chemical analyses (see below): for example, the higher water content found for the synthesised Ca-birnessite in comparison to vernadite is supported by the observation of stronger water bands in the IR spectrum of the former.

In all cases the very broad $\text{H}_2\text{O}/\text{OH}^-$ bands indicate that the water-related species randomly occupy a number of non-equivalent sites in the structures of the layered and tunnelled oxides.^[34] Furthermore, the intensity maxima for the bands between 3000 and 3600 cm^{-1} are always clearly above 3250 cm^{-1} and thus higher than expected for $\text{H}_2\text{O}/\text{OH}^-$ moieties that are part of well-defined hydrogen-bonding networks.^[35]

In summary, the XRD and IR datasets make it possible to roughly group the synthetic manganese oxides of this study into two groups: 1) crystalline “true oxides” (e.g., bixbyite, manganosite) with sharp XRD and IR signals, in which O^{2-} anions are the only oxygen-containing species and 2) MnO_x materials for which broad XRD signals and pronounced water IR bands are detected (e.g., hollandite, birnessite), both of which are typical features of less-ordered MnO_x materials containing a significant amount of randomly incorporated $\text{H}_2\text{O}/\text{OH}^-$ in addition to O^{2-} .

Table 2. Selected analytical data and WOC rates for the synthetic manganese oxides investigated in this study.

Mn oxide	Mn content [wt %] ^[a]	Av. Mn oxidation state ^[a]	S_{BET} [$\text{m}^2 \text{g}^{-1}$] ^[b]	WOC rate [$\text{mmolO}_2 \text{mol}_{\text{Mn}}^{-1} \text{h}^{-1}$]	WOC rate [$\mu\text{molO}_2 \text{m}^{-2} \text{h}^{-1}$]	Chemical formula
bixbyite	69.6 (69.6)	3.0 (3.0)	22 (24)	90	50 (50)	Mn_2O_3
hausmannite	71.2 (72.0)	2.7 (2.7)	11 (0.5)	0	0 (0)	Mn_3O_4
LiMn_2O_4	61.1 (60.7)	3.5 (3.5)	70 (14)	50	10 (40)	$\text{Li}_{0.92}\text{Mn}_2\text{O}_{3.50}$
marokite	52.2 (51.4)	2.9 (3.0)	1 (2.6)	30	285 (110)	$\text{Ca}_{0.48}\text{MnO}_{1.93}$
manganosite	80.1 (77.4)	2.0 (2.0–2.3)	2 (1.1)	0	0 (0)	$\text{MnO}_{1.05}$
pyrolusite	62.7 (63.2)	3.9 (4.0)	12 (10)	10	15 (20)	$\text{MnO}_{1.95} \cdot 0.1 \text{H}_2\text{O}$
ramsdellite ^[c]	61.6 (63.2)	3.7 (4.0)	95	425	50	$\text{MnO}_{1.85} \cdot 0.3 \text{H}_2\text{O}$
Cryptomelane	61.6 (43.5–63.2)	3.8 (3.0–4.0)	125	300	25	$\text{K}_{0.07}\text{MnO}_{1.94}$
hollandite ^[d]	58.7	3.9	80	275	40	$\text{MnO}_{1.95} \cdot 0.4 \text{H}_2\text{O}$
todorokite	48.7 (29.2–39.0)	3.5 (3.0–4.0)	250	1375	50	$\text{K}_{0.11}\text{Ca}_{0.22}\text{MnO}_{2.03} \cdot 0.7 \text{H}_2\text{O}$
birnessite	46.0 (38.5–39.1)	3.7 (3.7–4.0)	240	1650	60	$\text{Ca}_{0.21}\text{MnO}_{2.16} \cdot 1.3 \text{H}_2\text{O}$
vernadite	41.8 (53.9–68.7)	4.0 (3.8–4.0)	160	425	20	$\text{Na}_{0.15}\text{K}_{0.51}\text{MnO}_{2.25} \cdot 0.9 \text{H}_2\text{O}$

[a] In parentheses: typical values of naturally occurring mineral samples;^[14] [b] from N_2 sorption isotherms (in parentheses: calculated values S_{calcd} from particle sizes and densities; see the Supporting Information for details); [c] SEM and XRD suggest that the synthesised material contains significant amounts of birnessite impurities; [d] not a naturally occurring mineral.

Chemical composition

Using a previously established methodology, we next determined chemical formulae for the synthetic oxides by a combination of IC and redox titration (for details, see the Supporting Information and ref. [9]). The results for the different synthetic manganese oxides are listed in Table 2. A comparison between theoretical and experimentally determined Mn contents and oxidation states shows very good correlations for the crystalline 3D-network oxides bixbyite, hausmannite, LiMn_2O_4 , marokite and manganosite. In these cases the oxide phases indicated by XRD closely match the results of the chemical analysis.

Reasonable correlations between phase assignments by XRD and chemical formulae were also found for pyrolusite and ramsdellite, whose structures are characterised by small tunnels (types $[1 \times 1]$ and $[2 \times 1]$, respectively). These tunnels are too small to accommodate additional cations, which could be confirmed by IC, since only Mn^{2+} was found. On the other hand, these materials show some disorder (e.g., see the broad XRD peaks in Figure 2), and small amounts of water can apparently enter the structures (see IR spectra, Figure 3). In consequence, the manganese contents are in both cases slightly lower than the theoretical values and in agreement with formulae that contain 0.1–0.3 equivalents of H_2O per Mn.

For the oxides with wider tunnel geometries, such as cryptomelane ($[2 \times 2]$) and todorokite ($[3 \times 3]$), the cavities in the structure are large enough to accommodate both water and additional cations, especially M^{+2+} ions of alkali and alkaline earth metals, which are often present during syntheses in aqueous solution. This results in a large variety of possible cation and water contents, and thus complex chemical compositions are found. Often, the determined compositions differ significantly from those of the corresponding geologically occurring minerals. This compositional flexibility is known to be even more pronounced for layered oxides such as birnessite and vernadite (see above), and the data for the layered compounds listed in Table 2 reflect this very well.

In summary, the XRD, IR and chemical analyses of crystalline manganese oxides and MnO_x materials with structures containing narrow tunnels is rather straightforward and it is possible to confirm the isolation of the intended synthetic products with great certainty. On the other hand, the detectable differences in composition between the highly disordered MnO_x compounds birnessite, todorokite and vernadite are small, and thus an unambiguous assignment of the identities of the compounds without more expensive analytical tools such as X-ray absorption spectroscopy or X-ray photoelectron spectroscopy is difficult.^[8] However, for our set of samples a clear difference between the three products is the average manganese oxidation state, which is, as expected from the mineralogical data,^[14] found to be lowest for todorokite and highest for vernadite with an intermediate value for the birnessite sample. As the accuracy of this value obtained by our method is about ± 0.1 , the detected trend does not provide an ultimate proof, but at least a very good indication, that the chosen synthetic procedures indeed yielded the desired tunnelled or layered manganese oxides.

Morphology

Nitrogen sorption data, analysed by the BET method, were used to estimate the surface areas S_{BET} of the oxides. For the studied MnO_x series the measured values for S_{BET} vary over a large range of 1–250 $\text{m}^2 \text{g}^{-1}$ (Table 2), and S_{BET} is a parameter that is greatly influenced by the oxide type. In general, crystalline materials show (as expected) the smallest surface areas, and much larger S_{BET} values are found for tunnelled and especially layered oxides. To some degree surface areas correlate with crystallinity, but it is remarkable that even a rather well-ordered material such as hollandite (see XRD pattern in Figure 2) can show a high surface area of 80 $\text{m}^2 \text{g}^{-1}$.

The differences in surface areas might be explained by the nanostructured surfaces of the synthetic manganese oxides revealed by SEM (Figure 4). Again, the three oxide types also

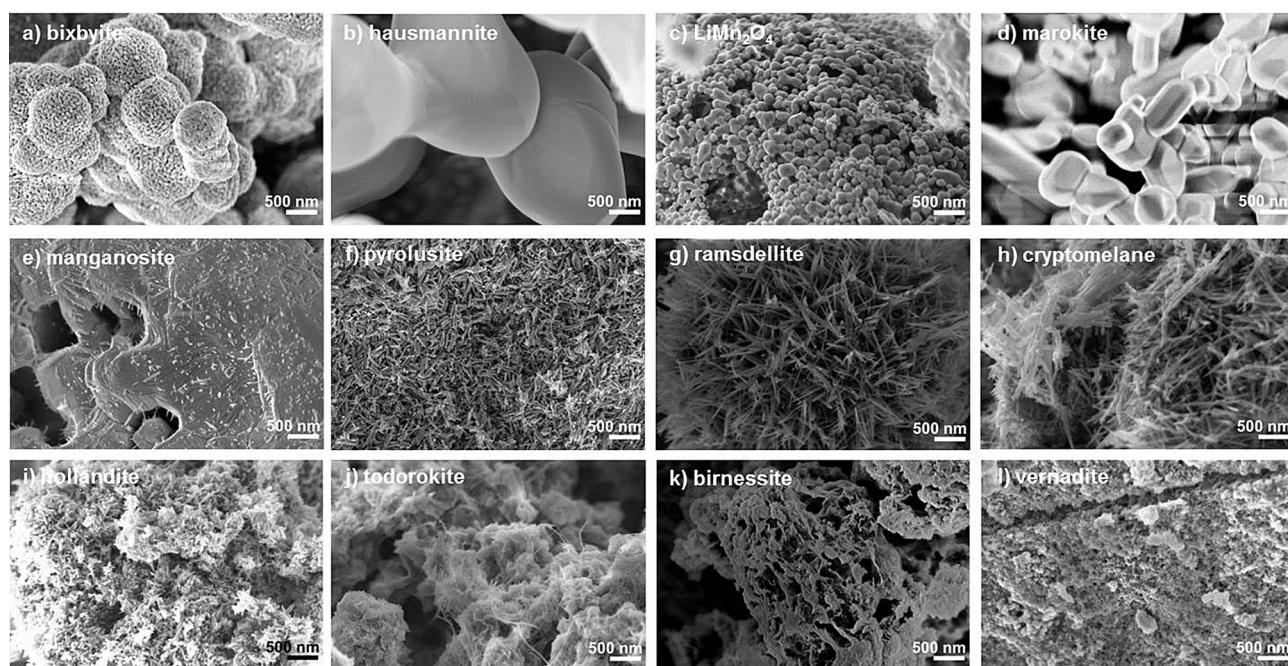


Figure 4. SEM images of different manganese oxides at the same magnification: a) bixbyite; b) hausmannite; c) LiMn_2O_4 ; d) marokite; e) manganosite; f) pyrolusite; g) ramsdellite; h) cryptomelane; i) cation-free hollandite; j) todorokite; k) birnessite; l) vernadite.

differ in this material property: tunnelled oxides can often be recognised by needle-like appearances (Figure 4 f–h), and because these needles are only few nanometres thick, large surface areas result (e.g., for cryptomelane). In contrast, crystalline materials such as bixbyite and hausmannite (Figure 4 a,b) consist of round, much larger particles with sizes of 0.5–10 μm . These are themselves sometimes built up from smaller spherical domains of 50–100 nm in diameter, as illustrated by the SEM image of LiMn_2O_4 (Figure 4 c).

The most irregular particle morphologies are found for the amorphous oxides todorokite, birnessite and vernadite (Figure 4 j–l). All are characterised by rather large grains (> 5 μm) that are aggregates of very fine ($d < 10$ nm) needles (todorokite) or irregular particles (birnessite, vernadite). Overall, non-compact, sponge-like structures are the result, especially well illustrated by the SEM image of birnessite (Figure 4 k).

The highly textured particle morphologies detected by SEM often correlate well with the S_{BET} values. Additionally, if the N_2 sorption data are analysed with regard to the porosity of the samples, one finds that most of the tunnelled and layered oxides are mesoporous materials with median pore diameters of about 15 nm (see the Supporting Information, Figure S4 and Table S2). The quite high surface areas of more than 100 m^2g^{-1} found especially for some of the samples synthesised by precipitation reactions can therefore be explained by the fact that the materials have pronounced surface textures and significant mesoporosity.

For the product of the synthesis of ramsdellite, we detected a mixture of two crystal forms by SEM: the fine needles typical of a tunnelled oxide, but also some sponge-like objects, which constitute about 10% of the material (Supporting Information, Figure S5). We suspect that these impurities are birnessite par-

ticles, since we found the broad peaks of birnessite in the XRD pattern and also detected a significantly lower average Mn oxidation state than expected from mineralogical data. However, additional cations (e.g., NH_4^+ ; see synthesis protocol) could not be detected, and therefore our impression from the SEM images that the material mainly consists of ramsdellite was confirmed.

From the presented analytical data, we conclude that compounds from all three MnO_x structure families were successfully synthesised. Manganese oxides of 3D-network structures show well-defined XRD patterns, chemical compositions very close to the theoretical values and consist of rather large particles with low surface areas. In contrast, tunnelled and layered oxides are generally much less ordered, more diverse in their chemical compositions and contain smaller particles with quite large surface areas of up to 250 m^2g^{-1} . We therefore find various aspects of diversity for this series of manganese oxides: chemical composition, Mn oxidation state, arrangement of the ions at the atomic level and different particle morphologies.

Water oxidation catalysis

The WOC activities of the synthetic manganese oxides were determined with Ce^{4+} as chemical oxidising agent. This reaction has been commonly used for this purpose in the past^[9,17,36] and is a good WOC screening method because: 1) Ce^{4+} is a strong (but not extreme) single-electron oxidant with an oxidation potential of about +1.6 V versus NHE;^[37] 2) ^{18}O labelling has shown that the oxygen formed in reactions of Ce^{4+} with MnO_x in water originates from the solvent and thus “true” water oxidation occurs^[38] and 3) solutions of Ce^{4+} are stable for hours, and thus extended catalysis runs can be

carried out.^[9] As a drawback, Ce^{4+} is only soluble under acidic conditions, and thus catalysis experiments are usually carried out at $\text{pH} \approx 2$.^[18,37]

As in our previous experiments,^[9] the synthetic oxides were suspended in air-saturated aqueous solutions of Ce^{4+} ($[\text{MnO}_x] = 1 \text{ mg mL}^{-1}$, $[\text{Ce}^{4+}] = 250 \text{ mM}$) in capped vials and kept at 40°C . Over 1 h, gas samples were taken from the headspace (air) every ten minutes and analysed by gas chromatography for their oxygen-to-nitrogen ratios. The amount of evolved oxygen can then be calculated from the increasing percentage of O_2 in the headspace above the catalytic mixture. The slightly elevated temperature was chosen to make comparisons with our earlier studies on water oxidation catalysis by manganese oxide possible, whereby the higher-than-ambient temperatures were a requirement of the previously used detection system.^[9,10] For further information on the catalysis experiments, see the Supporting Information and ref. [9].

The examples of typical oxygen-evolution traces in Figure 5 illustrate that, depending on the oxide, no (e.g., manganosite),

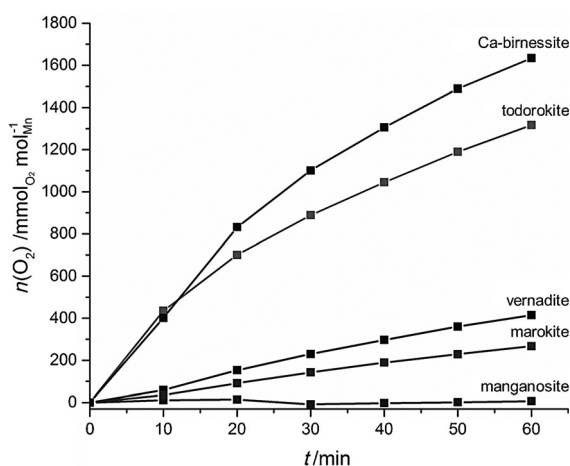


Figure 5. Exemplary oxygen evolution traces for reactions of Ce^{4+} with some of the synthetic manganese oxides prepared for this study. The additional O_2 accumulated in the headspace above the suspensions is plotted. Reaction conditions: 5 mL aqueous suspension, $[\text{MnO}_x] = 1 \text{ mg mL}^{-1}$, $[\text{Ce}^{4+}] = 250 \text{ mM}$, $T = 40^\circ\text{C}$.

slow (e.g., marokite) or much faster (e.g., todorokite) WOC is observed. The cases in which significant amounts of product are detected generally show no extended lag phase at the beginning of the experiment and some O_2 is detectable already at the first time of sampling ($t = 10 \text{ min}$). Furthermore, the traces for oxides with slow to intermediate rates show a constant WOC rate for the first hour, whereas fast catalysis (todorokite, birnessite) tends to slow down slightly with time. For birnessites, we have observed this behaviour before and confirmed that the rate decrease is not a result of MnO_x corrosion.^[9,10] Instead, we suspect that a combination of progressive Ce^{4+} consumption and the back-reaction of Ce^{3+} with O_2 might be reasons for this observation. As an example, for the fastest reaction rate found here (Ca-birnessite), one can calculate that about one quarter of the Ce^{4+} ions are consumed

during the monitored first hour of catalysis (see the Supporting Information). As a result, $[\text{Ce}^{4+}]$ is markedly decreased and significant $[\text{Ce}^{3+}]$ builds up, both possibly resulting in the slowing down of the rate of O_2 evolution after about 30 min that is observed in experiments with high WOC rates (Figure 5).

There are different options to analyse the data for comparison of WOC rates. The most common methods are calculations of the catalytic rate per unit mass, per mole of manganese ions and per unit surface area, and all of them have advantages and disadvantages. Because manganese centres are essential for WOC (at least in the absence of other potentially active metals such as Co, Ru and Ir, as is the case here), we (and others) have usually decided to plot the data per mole of Mn.^[9,19,21,36] This was also done here to generate the plots shown in Figure 5 or to derive the averaged rates for the first hour of reaction given in Figure 6 (top) and Table 2. In addition, comparisons per unit mass or per unit surface area are also shown (Figure 6 (bottom), Table 2 and the Supporting Information, Figure S6), and especially the surface-normalised values are discussed below.

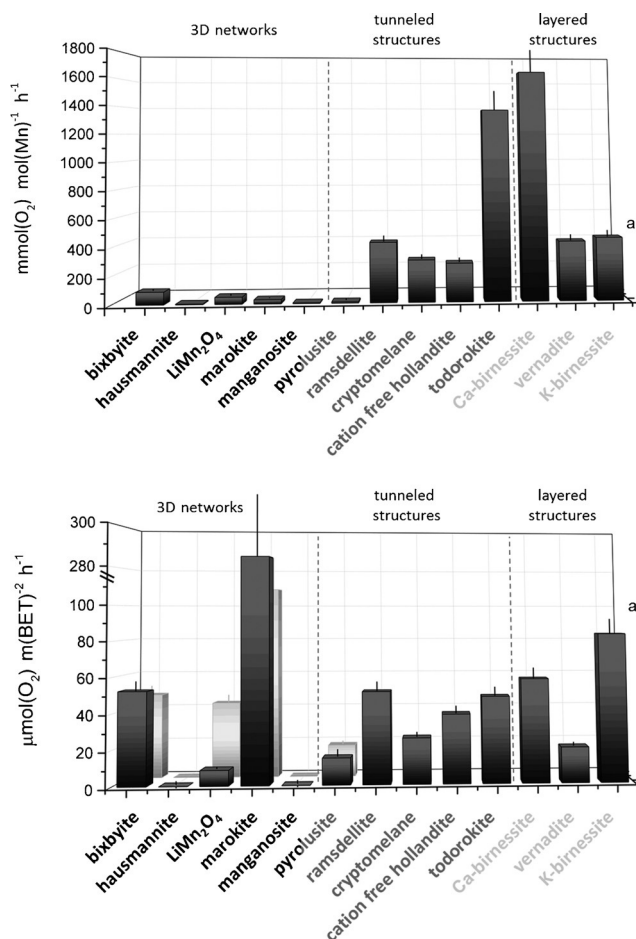


Figure 6. Comparison of catalytic water oxidation rates for the different oxides with Ce^{4+} as oxidant. Top: Data normalised per mole of Mn. Bottom: Rates per unit surface area determined by N_2 physisorption (front row, black) or calculated from particle sizes (back row, grey). Reaction conditions as in Figure 5. The error bars indicate the estimated 10% error of the absolute value. a) The values for potassium birnessite were taken from ref. [10].

As the main result of the catalysis data normalised per mole of Mn (Figure 6, top), we find two general trends for WOC by the different MnO_x : 1) most crystalline, 3D-network oxides show little or no activity in WOC and 2) for the groups of tunnelled and layered oxides, the best rates are clearly detected for todorokite and Ca-birnessite. In their respective groups of oxides, these are the two least-ordered materials. They show the highest surface areas/porosities and have accessible internal volumes due to their large tunnel diameters and interlayer spaces, respectively, and overall all these factors might explain the good catalytic performances of todorokite and Ca-birnessite.

The two above-mentioned general trends are most obvious when the data are normalised per manganese centre or per unit catalyst mass. If rates per unit surface area are compared, birnessite and todorokite still show very good rates, but three other oxides now also score very well: bixbyite, marokite and ramsdellite (Figure 6, bottom). These three thus also belong to the MnO_x showing good catalyst performance, and in the case of Mn_2O_3 this is in agreement with the data of Robinson et al.^[20] However, especially the first two of these materials belong to the group of crystalline oxides with small surface areas ($S_{\text{BET}} = 22$ and $1 \text{ m}^2 \text{ g}^{-1}$, respectively), and the accuracy of N_2 sorption measurements for such small values is low. To validate the S_{BET} values, we therefore also approximated specific surface areas by calculations in which theoretical densities from the crystal structures and (idealised) particle shapes from the SEM micrographs were used (see the Supporting Information for details). These calculated values S_{calcd} are also listed in Table 2, and for some materials, S_{calcd} and S_{BET} match rather well. For others, large differences are found, and as a result, the catalytic rates per surface areas can be very different depending on whether S_{BET} or S_{calcd} is used (Table 2 and Figure 6, bottom). Overall, this indicates that an analysis of catalytic rates per unit S_{BET} (though definitely important) is not very precise for materials of low surface areas.

What are the general properties emerging from these data that good MnO_x water oxidation catalysts have in common? We see at least four key points: 1) The oxidation state of manganese should allow changes between the critical oxidation states^[26] of +III and +IV while catalysis takes place. Hence, oxides that contain only Mn^{2+} (manganosite) or only Mn^{4+} (pyrolusite, hollandite) often perform poorly. In contrast, bixbyite, ramsdellite, cryptomelane, todorokite etc. also contain Mn^{3+} ions and therefore likely more active sites for water oxidation. 2) Incorporated ions and/or water can be beneficial for catalytic activity. Former studies revealed an important role for secondary cations in birnessites, in which (in analogy to PSII) Ca^{2+} leads to best catalytic results, followed by Sr^{2+} and K^+ (see difference between Ca and K birnessites in Figure 6, top, and the Supporting Information, Figure S6).^[10,13] The data presented here are in agreement with these previous conclusions, since the two fastest catalysts (per mole Mn or gramme) are again the two calcium-containing compounds of the series, Ca-birnessite and todorokite. More generally, it is striking that all oxides reaching rates greater than $200 \text{ mmol O}_2 \text{ mol}^{-1}_{\text{Mn}} \text{ h}^{-1}$ contain potassium or water in their structures, and thus we

conclude that, in addition to $\text{Mn}^{3+/4+}$ and O^{2-} , additional ions and/or water are also beneficial for obtaining a good Mn-based WOC material. However, we note that preliminary experiments indicated that the situation for mixed oxides appears to be very dynamic. As we found that cerium ions are able to replace some of the alkali/alkaline earth cations over time under "cerium conditions". From our initial data, this appears to be a rather complex process depending on oxide type, $[\text{Ce}^{4+}]$ and reaction time and thus requires further investigations beyond the scope of the present study. 3) For tunnelled oxides, the tunnel size influences catalytic activity, since larger diameters ($[2 \times 2]$ and especially $[3 \times 3]$) seem to be advantageous, even though the data for ramsdellite must be treated with caution, because this material contained birnessite impurities (see above). We suspect that large tunnel diameters make more active sites accessible for water oxidation, either because Ce^{4+} itself enters the structure or because injected holes move through the material and water molecules inside the tunnels are then oxidised.^[5,9,23,25] 4) WOC clearly depends on the crystallinity of the samples, since most of the best-performing materials are amorphous MnO_x with high specific surface areas. On the other hand, some crystalline materials such as marokite and bixbyite can also show impressive catalytic rates (at least per unit S_{BET}) if they fulfil some of the other advantageous criteria, such as incorporated Ca^{2+} and/or an intermediate Mn oxidation state of +III.

Conclusion

A series of manganese oxides has been investigated for use in WOC. The oxides can be classified according to their structural properties as 3D-network, tunnelled or layered materials. In addition to the arrangement of the ions at the atomic level, the three oxide families also differ when synthesis routes, crystallinities and particle morphologies are compared. For the rates of WOC with Ce^{4+} as oxidant, we found a general reactivity trend of 3D networks < tunnelled structures \approx layered structures. Interestingly, this is in agreement with a related (but very limited) first study by us on electrocatalytic water oxidation with three different MnO_x , for which a ranking Ca-birnessite > Mn_2O_3 > MnO_2 was found when anodes coated by these oxides were used for water electrolysis at pH 7.^[39] Given the large differences in catalytic performance found here, we will now carry out a similar screening to assess the suitability of the different MnO_x for water-oxidation electrocatalysis. Because electrochemical water-oxidation rates strongly depend on parameters such as pH and oxidation potential, but also oxide conductivity,^[8] a comparison of the Ce^{4+} and electrolysis datasets will likely offer interesting insights into the catalytic process.

Overall, we firstly conclude that good WOC activity is found for amorphous materials containing highly flexible Mn–O linkages. Secondly, the structures should offer room for additional cations and/or water, since water oxidation most probably takes place not only on the particle surfaces, but also in tunnels or between $[\text{MnO}_6]$ layers. Finally, two crystalline oxides (bixbyite and marokite) also showed surprisingly high catalytic

activities per unit surface area, and future studies should attempt to synthesise such oxides in nanostructured forms. If WOC activities per unit area remain unaltered, these crystalline materials may prove to be an alternative to the MnO_x water oxidation catalysts with layered or wide-tunnelled structures, which are otherwise the clear winners of the above-presented screening.

Experimental Section

General considerations

All reagents and solvents were purchased from commercial sources and were used without further purification. Deionised water was used for all experiments and, unless otherwise stated, all syntheses described below were carried out in aqueous solutions. The sample of manganosite (MnO) was obtained from ChemPur. For centrifugation we used a Universal 320 centrifuge from Hettich Zentrifugen. If not stated otherwise, centrifugation was carried out for 2 min at 3000 rpm. For details of analytical procedures and catalysis runs to probe WOC activity, see the Supporting Information and ref. [9].

Experimental details and analytical procedures

Infrared spectroscopy: IR spectra of the neat solid compounds were measured with a Thermo Scientific Nicolet iS10 FTIR spectrometer equipped with a diamond ATR unit.

Powder XRD: Powder XRD patterns were recorded in reflection geometry with a Seifert 3003 TT instrument and $\text{Cu}_{K\alpha}$ radiation. Oxide powders were mounted on aluminium frames exposing an area of about 4 cm^2 of the MnO_x powders to the X-ray beam, which hit the sample at an incident angle of 1° .

BET analysis: N_2 physisorption isotherms were measured with a Thermo Porotec Sorptomatic 1990 instrument and analysed according to the BET theory to determine S_{BET} . Pore volumes and diameters were calculated with the data analysis software Sorptomatic provided by Thermo and are listed in the Supporting Information (Table S2) together with general porosity types according to ref. [40]. Prior to analysis, oxide samples were heated at 150°C for 5 h and about 10^{-5} bar. For water-containing samples, post-measurement IR spectra indicated that this treatment does not result in significant loss of intercalated H_2O molecules. As N_2 physisorption does not result in very accurate data for $S_{\text{BET}} < 20 \text{ m}^2 \text{ g}^{-1}$, we additionally approximated surface areas for samples of low S_{BET} from the particle sizes detectable by SEM (see the Supporting Information).

SEM and EDX measurements: SEM imaging and energy-dispersive X-ray (EDX) analysis of the oxides were performed with a LEO 1525 scanning electron microscope at 3 kV accelerating voltage.

Ion chromatography: Contents of manganese, calcium, potassium, sodium and lithium ions were determined with a Metrohm 882 Compact IC plus ion chromatograph equipped with a Metrosep C4 150/4 column and a conductivity detector. A solution of dipicolinic acid (0.75 mM) and nitric acid (2 mM) served as IC eluent, and the chromatograph was calibrated with AAS standard solutions (Roth). Prior to analysis, the oxide samples (ca. 10 mg) were treated with 1 mL of concentrated $\text{HNO}_3/30\% \text{ H}_2\text{O}_2$ (1/10), which completely dissolved the oxide and converted all manganese to its Mn^{2+} form. The solutions were then diluted to 250 mL, and 20 μL samples were injected into the IC system.

Determination of the average manganese oxidation state by redox titration: The method followed an established procedure for the quantification of MnO_2 .^[41] Carefully weighed samples of the oxides (100–150 mg) were mixed with a solution of sodium oxalate (10 mL, 0.2 M) and sulfuric acid (10 mL, 0.5 M). The solution was stirred at 60°C until all oxide had dissolved. In this step manganese is quantitatively reduced to its Mn^{2+} form. In the following, the excess of oxalate was determined by titration of the remaining oxalate with a solution of KMnO_4 . In combination with the manganese content of the material (determined by IC; see above), the average oxidation state of the manganese centres could then be calculated.

Oxygen detection by GC: To determine the concentration of oxygen in the headspace of the reaction vessels, gas chromatograms were recorded. We used a PerkinElmer Clarus 480 gas chromatograph with a 12 ft. \times 1/8 in. 5 \AA Molsieve column (Restek). The carrier gas was helium, the GC oven temperature was set to 70°C and O_2 and N_2 were quantified by a thermal conductivity detector (TCD). Ambient air served as calibration gas.

Determination of WOC rates for experiments with Ce^{IV} : The method followed a previously developed procedure.^[9] Precisely weighed oxide samples (ca. 5 mg) and $(\text{NH}_4)_2\text{Ce}(\text{NO}_3)_6$ (685 mg, 1.25 mmol) were filled into 20 mL septum vials. After addition of 5 mL of air-saturated water, the vials were capped immediately with gas-tight septa and sonicated for 20 s. The reaction containers were kept at 40°C in a water bath, and headspace gas samples (100 μL) were injected into the gas chromatograph by hand with a gas-tight syringe (Hamilton). Six injections at 10 min intervals were carried out. The amount of oxygen evolved was then calculated for each headspace extract from the detected O_2/N_2 signal ratios. To do so, the amount of oxygen from air (corresponding to the detected nitrogen peak) was calculated and subtracted to leave the excess of O_2 generated by the water-oxidation reaction. We estimate the error margin for the rate determination to be in the range of $\pm 10\%$, as is indicated by error bars in Figure 6. For more information, see the supporting information of Frey et al.^[9]

Syntheses of manganese oxides

Bixbyite: Analogous to the literature procedure,^[27] MnCO_3 (4.19 g) was heated to 600°C for 24 h in air. Yield: 98%.

Hausmannite: The synthesis of hausmannite was adapted from ref. [27]. MnCO_3 (6.73 g) was heated to 1000°C for 24 h in air. Yield: 89%.

LiMn_2O_4 : LiMn_2O_4 was prepared via a sol-gel route according to the procedure established by Vivekanandhan et al.^[28] A solution of citric acid (28.8 g, 150 mmol) and urea (9.01 g, 150 mmol) in water (100 mL) was added dropwise to a solution of LiNO_3 (1.72 g, 2.5 mmol) and $\text{Mn}(\text{OAc})_2 \cdot 4\text{H}_2\text{O}$ (12.3 g, 5.00 mmol) in water (100 mL). Concentrated HNO_3 (20 mL) was then added slowly with stirring. The water was evaporated completely with a rotary evaporator and the yellow precipitate was heated to 170°C for 12 h. Subsequently, the brown, sponge-like solid was calcined twice at 350°C for 12 h. The product was ground with a pestle and mortar after each calcination step. Yield: 77%.

Marokite: Marokite has been previously synthesised by us.^[17] $\text{Ca}(\text{NO}_3)_2 \cdot 4\text{H}_2\text{O}$ (0.473 g, 2.00 mmol) and $\text{Mn}(\text{NO}_3)_2 \cdot 4\text{H}_2\text{O}$ (0.703 g, 2.80 mmol) were dissolved in water (5 mL). A solution of KMnO_4 (0.190 g, 1.20 mmol) and KOH (8.40 g, 150 mmol) in water (10 mL) was added dropwise with vigorous stirring within 15 min. The suspension was allowed to react for another 15 min. The dark-brown precipitate was separated by centrifugation and washed with water ($5 \times 200 \text{ mL}$) and centrifuged again. The crude product was

then dried at 60 °C for 6 h and calcined at 1000 °C for 10 h. Yield: 87%.

Pyrolusite: The synthesis was adapted from Ghodbane et al.^[29] First, a lithium-doped birnessite was synthesised: Mn(OAc)₂·4H₂O (3.92 g, 16.0 mmol) in water (30 mL) was added with stirring to a solution of KOH (10.1 g) in water (30 mL). A solution of KMnO₄ (0.949 g, 6.00 mmol) in water (100 mL) was added dropwise with vigorous stirring to form a brown suspension. The mixture was allowed to age for 2 h with gentle stirring, after which the crude product was obtained by centrifugation. The supernatant was discarded and the precipitate was suspended in water (200 mL) and again centrifuged. This washing procedure was carried out seven times in total. The product was then suspended in an aqueous solution of LiCl (1 molL⁻¹, 200 mL) and the suspension was stirred for 24 h. The suspension was centrifuged and the centrifugate washed with water (200 mL), after which it was separated by centrifugation again. This cation exchange was repeated once more. The brown precipitate was dried at 60 °C for 24 h. Part of this lithium-doped birnessite (ca. 400 mg) was suspended in a solution of H₂SO₄ (0.5 molL⁻¹) and LiCl (1 molL⁻¹) in water (10 mL). The suspension was transferred to a Teflon-lined autoclave (15 mL) and heated to 150 °C for 48 h. The dark-brown precipitate was separated by centrifugation, washed with water (3×50 mL), and centrifuged again. The dark brown product was then dried at 60 °C for 48 h. Yield: 64%.

Ramsdellite: This synthesis was adapted from Ghodbane et al.^[29] MnSO₄·4H₂O (0.423 g, 2.50 mmol) and (NH₄)₂S₂O₈ (0.571 g, 2.50 mmol) were dissolved in water (8 mL) and the solution was transferred to a Teflon-lined autoclave (15 mL). The solution was heated to 85 °C for 12 h. The dark-brown crude product was separated by centrifugation, washed with water (50 mL) and centrifuged again. This washing procedure was repeated twice. The product was then dried at 70 °C for 72 h. Yield: 66%.

Cryptomelane: This oxide was prepared by following a procedure developed by Luo et al.^[30,31] KMnO₄ (6.01 g, 38.0 mmol) in water (30 mL) was added dropwise to a solution of MnSO₄·H₂O (10.1 g, 60.0 mmol) and HNO₃ (3 mL) in water (100 mL) at 110 °C. The brown suspension was heated to reflux for 24 h. The crude brown product was obtained by centrifugation. The colourless supernatant was discarded and the precipitate was suspended in water (200 mL) and again centrifuged. This washing procedure was carried out five times in total. The greyish black precipitate was dried at 120 °C for 12 h and ground into fine powder with a pestle and mortar. Yield: 98%.

Cation-free hollandite: This synthesis was developed by Johnson et al.^[32] and modified by Robinson et al.^[20] Mn₂O₃ (bixbyite, 2.05 g, 13.0 mmol; see above) was heated to 700 °C for 12 h to remove impurities. The residue was added to an aqueous solution of H₂SO₄ (4 molL⁻¹) and stirred at 80 °C for 6 h. After the suspension was allowed to cool the crude product was obtained by centrifugation. The supernatant was discarded and the precipitate was suspended in water (200 mL) and centrifuged. This washing procedure was carried out three times in total. The brown precipitate was dried at 90 °C for 16 h. Yield: 93%.

Todorokite: The preparation was carried out by following a publication by Luo et al.^[15] A solution of Mn(OAc)₂·4H₂O (0.784 mg, 3.20 mmol) and Ca(OAc)₂·H₂O (0.163 mg, 0.925 mmol) in water (5 mL) was added dropwise to a solution of KOH (2.90 g, 51.7 mmol) in water (6 mL). KMnO₄ (0.190 mg, 1.20 mmol) was added slowly with vigorous stirring. The brown suspension was allowed to age for 1 h. The crude product was obtained by centrifugation, re-suspended in water (10 mL) and filled into a Teflon-lined autoclave (15 mL). The mixture was then heated to 150 °C for 48 h.

The precipitate was obtained by centrifugation. The brown product was dried at room temperature. Yield: 98%.

Birnessite: For the synthesis of a Ca-birnessite a well-established route was used that was developed by Suib et al.^[15,42] and modified by us.^[9,10] Three solutions were prepared: solution A: KOH (14.4 g, 250 mmol) in H₂O (30 mL); solution B: Mn(OAc)₂·4H₂O (3.92 g, 16.0 mmol) and Ca(OAc)₂·H₂O (0.846 g, 4.80 mmol) in H₂O (30 mL); solution C: KMnO₄ (0.948 g, 6.00 mmol) in H₂O (100 mL). First solution B was added dropwise over 10 min with stirring to solution A to give an off-white to light brown suspension. Then, solution C was added dropwise to the vigorously stirred mixture in 30 min. After gently stirring the resulting dark brown to black suspension for 2 h at room temperature, the crude product was obtained by centrifugation. The supernatant was discarded, and the precipitate was suspended in H₂O and again centrifuged. This washing procedure was carried out seven times in total. The precipitate was dried at 60 °C for 48 h. Yield: 95%.

Vernadite: This synthesis was adapted from Villalobos et al.^[33] As described in the synthesis of birnessite three solutions were prepared: solution A: NaOH (2.78 g, 69.5 mmol) in H₂O (130 mL); solution B: KMnO₄ (4.00 g, 25.3 mmol) in H₂O (180 mL); solution C: MnCl₂·4H₂O (7.52 g, 3.80 mmol) in H₂O (130 mL). First, solution B was added over 5 min to solution A with stirring. Subsequently, solution C was added to the mixture over 20 min with vigorous stirring. The brown suspension was allowed to age with gentle stirring for 30 min, after which the precipitate was allowed to settle down for 2 h. The light-brown supernatant was discarded. The obtained crude product was re-suspended in water (90 mL) and centrifuged. The obtained brown product was dried at room temperature for 72 h. Yield: 91%.

Acknowledgements

At the ALU Freiburg, we would like to thank Katrin Kaspar for obtaining SEM images, Sabine Zuelsdorf and Simon Rudolf for assistance with the chemical analyses, Andreas Warmbold for BET measurements and Robin White for advice on the analysis of sorption isotherms. The Freiburger Materialforschungszentrum (FMF) granted access to its XRD instrument. This work was financially supported by the Deutsche Forschungsgemeinschaft (DFG projects KU 2885/1-1 and KU 2885/2-1, the latter part of the priority program SPP 1613).

Keywords: heterogeneous catalysis · manganese · oxidation · oxides · water splitting

- [1] a) REN21 Renewable Energy Policy Network, *Renewables 2014 Global Status Report*; b) A. Thapper, S. Styring, G. Saracco, A. W. Rutherford, B. Robert, A. Magnuson, W. Lubitz, A. Llobet, P. Kurz, A. Holzwarth, S. Fiechter, H. de Groot, S. Campagna, A. Braun, H. Bercegol, V. Artero, *Green* **2013**, *3*, 43–57.
- [2] J. Barber, *Chem. Soc. Rev.* **2009**, *38*, 185–196.
- [3] M. Suga, F. Akita, K. Hirata, G. Ueno, H. Murakami, Y. Nakajima, T. Shimizu, K. Yamashita, M. Yamamoto, H. Ago, J.-R. Shen, *Nature* **2014**, *517*, 99–103.
- [4] a) N. Cox, D. A. Pantazis, F. Neese, W. Lubitz, *Acc. Chem. Res.* **2013**, *46*, 1588–1596; b) P. E. Siegbahn, *Acc. Chem. Res.* **2009**, *42*, 1871–1880.
- [5] H. Dau, C. Limberg, T. Reier, M. Risch, S. Roggan, P. Strasser, *ChemCat-Chem* **2010**, *2*, 724–761.
- [6] T. S. Glikman, I. S. Shchegoleva, *Kinet. Katal.* **1968**, *9*, 461–462.
- [7] V. Y. Shafirovich, N. K. Khannanov, A. E. Shilov, *J. Inorg. Biochem.* **1981**, *15*, 113–129.

- [8] P. Kurz, *Topics Curr. Chem.* **2015**, DOI: 10.1007/128_2015_634.
- [9] C. E. Frey, M. Wiechen, P. Kurz, *Dalton Trans.* **2014**, 43, 4370.
- [10] M. Wiechen, I. Zaharieva, H. Dau, P. Kurz, *Chem. Sci.* **2012**, 3, 2330–2339.
- [11] F. Jiao, H. Frei, *Chem. Commun.* **2010**, 46, 2920–2922.
- [12] A. Iyer, J. Del-Pilar, C. K. King'ondeu, E. Kissel, H. F. Garces, H. Huang, A. M. El-Sawy, P. K. Dutta, S. L. Suib, *J. Phys. Chem. C* **2012**, 116, 6474–6483.
- [13] M. M. Najafpour, D. J. Sedigh, B. Pashaei, S. Nayeri, *New J. Chem.* **2013**, 37, 2448.
- [14] J. E. Post, *Proc. Natl. Acad. Sci. USA* **1999**, 96, 3447–3454.
- [15] J. Luo, Q. H. Zhang, A. M. Huang, O. Giraldo, S. L. Suib, *Inorg. Chem.* **1999**, 38, 6106–6113.
- [16] I. Zaharieva, M. M. Najafpour, M. Wiechen, M. Haumann, P. Kurz, H. Dau, *Energy Environ. Sci.* **2011**, 4, 2400–2408.
- [17] M. M. Najafpour, T. Ehrenberg, M. Wiechen, P. Kurz, *Angew. Chem. Int. Ed.* **2010**, 49, 2233–2237; *Angew. Chem.* **2010**, 122, 2281–2285.
- [18] A. Harriman, I. J. Pickering, J. M. Thomas, P. A. Christensen, *J. Chem. Soc. Faraday Trans. 1* **1988**, 84, 2795–2806.
- [19] V. Boppa, B. Ram, F. Jiao, *Chem. Commun.* **2011**, 47, 8973–8975.
- [20] D. M. Robinson, Y. B. Go, M. Mui, G. Gardner, Z. Zhang, D. Mastrogiiovanni, E. Garfunkel, J. Li, M. Greenblatt, G. C. Dismukes, *J. Am. Chem. Soc.* **2013**, 135, 3494–3501.
- [21] M. Fekete, R. K. Hocking, S. L. Y. Chang, C. Italiano, A. F. Patti, F. Arena, L. Spiccia, *Energy Environ. Sci.* **2013**, 6, 2222.
- [22] Y. Okuno, O. Yonemitsu, Y. Chiba, *Chem. Lett.* **1983**, 815–818.
- [23] Y. Gorlin, B. Lassalle-Kaiser, J. D. Benck, S. Gul, S. M. Webb, V. K. Yachandra, J. Yano, T. F. Jaramillo, *J. Am. Chem. Soc.* **2013**, 135, 8525–8534.
- [24] B. M. Tebo, J. R. Bargar, B. G. Clement, G. J. Dick, K. J. Murray, D. Parker, R. Verity, S. M. Webb, *Annu. Rev. Earth Planet. Sci.* **2004**, 32, 287–328.
- [25] G. Elmaci, C. E. Frey, P. Kurz, B. Zümreoğlu-Karan, *Inorg. Chem.* **2015**, 54, 2734–2741.
- [26] P. Rasiyah, A. C. Tseung, *J. Electrochem. Soc.* **1984**, 131, 803–808.
- [27] I. Ursu, R. Alexandrescu, I. N. Mihailescu, I. Morjan, V. Jianu, C. Popescu, *J. Phys. D* **1986**, 19, 1183.
- [28] S. Vivekanandhan, M. Venkateswarlu, N. Satyanarayana, *J. Alloys Compd.* **2007**, 441, 284–290.
- [29] O. Ghodbane, J.-L. Pascal, B. Fraise, F. Favier, *ACS Appl. Mater. Interfaces* **2010**, 2, 3493–3505.
- [30] S. Luo, L. Duan, B. Sun, M. Wei, X. Li, A. Xu, *Appl. Catal. B* **2015**, 164, 92–99.
- [31] A. Iyer, H. Galindo, S. Sithambaram, C. King'ondeu, C.-H. Chen, S. L. Suib, *Appl. Catal. A* **2010**, 375, 295–302.
- [32] C. S. Johnson, D. W. Dees, M. F. Mansuetto, M. M. Thackeray, D. R. Vissers, D. Argyriou, C.-K. Loong, L. Christensen, *J. Power Sources* **1997**, 68, 570–577.
- [33] M. Villalobos, B. Toner, J. Bargar, G. Sposito, *Geochim. Cosmochim. Acta* **2003**, 67, 2649–2662.
- [34] R. M. Potter, G. R. Rossman, *Am. Mineral.* **1979**, 64, 1199–1218.
- [35] K. Nakamoto, *Infrared and Raman Spectra of Inorganic and Coordination Compounds*, Wiley, Hoboken, NJ, **2009**.
- [36] M. M. Najafpour, B. Pashaei, S. Nayeri, *Dalton Trans.* **2012**, 41, 4799–4805.
- [37] A. F. Holleman, E. Wiberg, *Lehrbuch der Anorganischen Chemie*, De Gruyter, Berlin, **2007**.
- [38] D. Shevela, S. Koroidov, M. M. Najafpour, J. Messinger, P. Kurz, *Chem. Eur. J.* **2011**, 17, 5415–5423.
- [39] S. Y. Lee, D. González-Flores, J. Ohms, T. Trost, H. Dau, I. Zaharieva, P. Kurz, *ChemSusChem* **2014**, 7, 3442–3451.
- [40] J. Rouquerol, D. Avnir, C. W. Fairbridge, D. H. Everett, J. M. Haynes, N. Pernicone, J. D. F. Ramsay, K. S. W. Sing, K. K. Unger, *Pure Appl. Chem.* **1994**, 66, 1739–1758.
- [41] G. Jander, K. F. Jahr, G. Schulze, J. Simon, *Maßanalyse: Theorie und Praxis der Titrations mit chemischen und physikalischen Indikationen*, De Gruyter, Berlin, **2003**.
- [42] J. Luo, Q. Zhang, S. L. Suib, *Inorg. Chem.* **2000**, 39, 741–747.

Received: April 8, 2015

Published online on September 1, 2015